nature neuroscience

ARTICLES

Saltatory remodeling of *Hox* chromatin in response to rostrocaudal patterning signals

Esteban O Mazzoni[1–4,10], Shaun Mahony[5,6,10], Mirza Peljto[1–3,9,10], Tulsi Patel[1–3], Seraphim R Thornton[7], Scott McCuine[8], Christopher Reeder[5], Laurie A Boyer[7], Richard A Young[8], David K Gifford[5] & Hynek Wichterle[1–3]

Hox **genes controlling motor neuron subtype identity are expressed in rostrocaudal patterns that are spatially and temporally collinear with their chromosomal organization. Here we demonstrate that *Hox* chromatin is subdivided into discrete domains that are controlled by rostrocaudal patterning signals that trigger rapid, domain-wide clearance of repressive histone H3 Lys27 trimethylation (H3K27me3) polycomb modifications. Treatment of differentiating mouse neural progenitors with retinoic acid leads to activation and binding of retinoic acid receptors (RARs) to the *Hox1–Hox5* chromatin domains, which is followed by a rapid domain-wide removal of H3K27me3 and acquisition of cervical spinal identity. Wnt and fibroblast growth factor (FGF) signals induce expression of the Cdx2 transcription factor that binds and clears H3K27me3 from the *Hox1–Hox9* chromatin domains, leading to specification of brachial or thoracic spinal identity. We propose that rapid clearance of repressive modifications in response to transient patterning signals encodes global rostrocaudal neural identity and that maintenance of these chromatin domains ensures the transmission of positional identity to postmitotic motor neurons later in development.**

Development of a functional CNS relies on mechanisms that assign precise positional identity to dividing neural progenitors. Signaling factors released from localized sources within the embryo subdivide the nascent neural tube along two principal axes: dorsoventral and rostrocaudal. Rostrocaudal patterning is established in early neural progenitors at around the time of neural tube closure[1] and manifests in the developing hindbrain and spinal cord through the differential expression of a phylogenetically conserved family of Hox transcription factors[1–5]. Although the activity of rostrocaudal patterning signals is transient, it has a lasting effect on the pattern of *Hox* gene expression that is maintained for the rest of embryonic development[1]. Maintenance of *Hox* gene expression is crucial for the generation of segment-specific types of spinal nerve cells, including columnar and pool-specific motor neuron subtypes that are necessary for the proper wiring and functionality of spinal motor circuits[2–4].

Mechanisms that control the establishment and maintenance of *Hox* gene expression have been under intense scrutiny. Mouse *Hox* genes are organized into four chromosomal clusters, each of which harbors a subset of 13 paralogous *Hox* genes. Individual genes within these clusters are expressed in patterns that are spatially and temporally collinear with their physical chromosomal organization[6,7]. Mutations in the polycomb group (PcG) complex of histone-modifying enzymes lead to defects in the maintenance of *Hox* gene expression[8,9], indicating that histone modifications and chromatin remodeling are important in rostrocaudal patterning. *Hox* chromatin is found in a compacted and repressed state in pluripotent embryonic stem cells (ESCs)[10] that is characterized by a high density of H3K27me3 deposited by the polycomb repressive complex 2 (PRC2)[11,12]. The distribution of H3K27me3 modifications is altered during embryonic development, resulting in a clearance of repressive modifications from chromatin domains harboring transcribed *Hox* genes[13–15]. On the basis of a correlation between chromatin modifications and *Hox* gene expression, it has been proposed that progressive removal of the repressive modifications from *Hox* chromatin controls the temporally progressive collinear pattern of *Hox* gene expression[14].

Rostrocaudal patterning of the embryo is controlled by diffusible patterning signals. Specification of cervical, brachial and thoracic spinal-cord identity depends on opposing gradients of retinoic acid and FGF signals[5,16–18]. Retinoic acid secreted by the paraxial mesoderm activates RARs bound to genomic sites and initiates the recruitment of additional RARs within *Hox* chromatin domains harboring *Hox1–Hox5* paralog genes[19]. FGF signaling activates the expression of more caudal *Hox6–Hox9* paralog genes, which control brachial and thoracic spinal identity[5,16–18]. The caudal-type homeobox protein Cdx2 is a candidate transcription factor linking FGF signaling to the regulation of caudal brachial and thoracic identity[18]. Wnt and FGF signals jointly induce the expression of Cdx2 (refs. 20–22), and Cdx2

[1]Department of Pathology and Cell Biology, Center for Motor Neuron Biology and Disease, Columbia Stem Cell Initiative, Columbia University Medical Center, New York, New York, USA. [2]Department of Neurology, Columbia University Medical Center, New York, New York, USA. [3]Department of Neuroscience, Columbia University Medical Center, New York, New York, USA. [4]Department of Biology, New York University, New York, New York, USA. [5]Computer Science and Artificial Intelligence Laboratory, Massachusetts Institute of Technology, Cambridge, Massachusetts, USA. [6]Department of Biochemistry and Molecular Biology, Center for Eukaryotic Gene Regulation, The Pennsylvania State University, University Park, Pennsylvania, USA. [7]Department of Biology, Massachusetts Institute of Technology, Cambridge, Massachusetts, USA. [8]Whitehead Institute for Biomedical Research, Cambridge, Massachusetts, USA. [9]Present address: Flagship Biosciences, Boulder, Colorado, USA. [10]These authors contributed equally to this work. Correspondence should be addressed to E.O.M. (eom204@nyu.edu), H.W. (hw350@columbia.edu) or D.K.G. (gifford@mit.edu).

Received 22 March; accepted 10 July; published online 18 August 2013; doi:10.1038/nn.3490

binding sites have been identified in a *cis*-regulatory element that is located between *Hoxc8* and *Hoxc9* (ref. 23).

To study the dynamic interactions between extrinsic signals and changes in chromatin architecture during rostrocaudal patterning, we developed an *in vitro* differentiation system that faithfully recapitulates the normal development of cervical and brachiothoracic spinal motor neurons. We provide evidence that patterning signals specifying cervical and brachiothoracic identity activate RARs and Cdx2 transcription factors that are recruited to distinct *Hox* chromatin domains. We demonstrate that this pattern of repressive H3K27me3 modifications is rapidly altered after exposure to rostrocaudal patterning signals. The repressive modifications are cleared from *Hox* chromatin domains occupied by RARs or Cdx2 transcription factors in a domain-wide saltatory process instead of the proposed temporally progressive directional process. We conclude that changes in H3K27me3 chromatin modifications are controlled by transient patterning signals and that stable maintenance of repressed and accessible *Hox* chromatin domains from progenitors to postmitotic motor neurons encodes the positional identity of differentiating cells and ensures proper specification of motor neuron subtype identity. On the basis of our findings, we propose a comprehensive model of rostrocaudal patterning that integrates the effects of extrinsic patterning signals, the activation of developmentally regulated transcription factors and changes in *Hox* chromatin modifications during neural development.

RESULTS

Domain-wide changes in *Hox* chromatin modifications

To characterize the mechanisms underlying the establishment and maintenance of the rostrocaudal pattern of *Hox* gene expression, we examined molecular mechanisms leading to the specification of spinal motor neurons with distinct rostrocaudal positional identities. We used an *in vitro* differentiation system of mouse ESCs to spinal motor neurons that recapitulates normal motor neuron development in a highly homogeneous neural context[24]. This system eliminates the potentially confounding influences of mesodermal and endodermal lineages in the developing embryo. The high yield and efficiency of motor neuron differentiation makes this system amenable to analysis of temporal changes in chromatin modifications by chromatin immunoprecipitation (ChIP) analysis[25]. ESCs are converted to cervical spinal motor neurons by joint exposure of cells on day 2 of differentiation to retinoic acid and a ventralizing sonic hedgehog signaling agonist (smoothened agonist, SAG)[24]. Retinoic acid treatment triggers the recruitment of RARs to genomic sites localized within the 3′ ends of *Hox* clusters[19], leading to the specification of rostral cervical motor neurons expressing Hox4 and Hox5 transcription factors from paralogous groups A and C by day 6 of differentiation[16,24] (**Fig. 1a**).

To understand how retinoic acid signaling is translated into a developmentally stable pattern of *Hox* gene expression, we examined changes in the distribution of repressive PcG-mediated histone H3 modifications (H3K27me3) that have been previously implicated

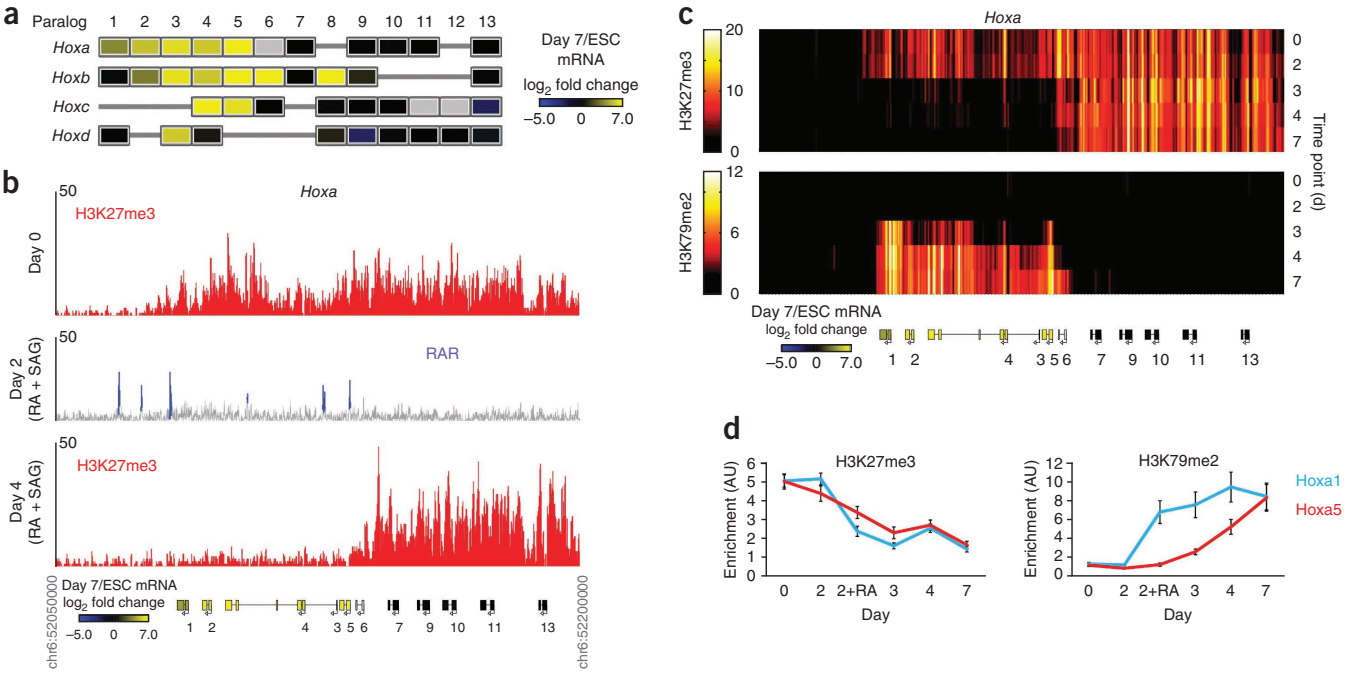

Figure 1 Domain-wide clearance of repressive histone modifications and changes in *Hox* gene expression in response to retinoic acid. (**a**) Expression profiling of ESCs and day-7 retinoic acid and SAG-treated embryoid bodies differentiated into motor neurons. Retinoic acid treatment induces rostral *Hox1*–*Hox5* gene expression (yellow). The color indicates the $\log_2$ fold change in signal intensity between ESCs and day-7 differentiated cells. Genes in gray are not represented on the GeneChip arrays. (**b**) *Hoxa* chromatin is parceled during motor neuron differentiation into two domains that are distinguished by different densities of H3K4me3 and H3K27me3 modifications. The red tracks represent H3K27me3 enrichment over a 150-kb genomic region spanning the *Hoxa* cluster at days 0 (ESCs) and 4 (progenitors). The blue peaks represent RAR binding 8 h after treatment with retinoic acid and SAG (RA + SAG) on day 2 (ref. 19). The color of the genes indicates the $\log_2$ fold change in signal intensity between ESCs and day 7. (**c**) Rapid and synchronous removal of H3K27me3 modifications from the *Hoxa1*–*Hoxa5* domain. The heat map represents enrichment of the H3K27me3 and H3K79me2 modifications along the *Hoxa* cluster at five time points during motor neuron differentiation. (**d**) Temporal changes in H3K79me2 and H3K27me3 modifications over *Hoxa1* and *Hoxa5*. The values reflect the average enrichment of modifications over 1-kb genomic regions flanking transcription start sites (TSSs). There was delayed accumulation of H3K79me2 modifications in *Hoxa5* (marking actively transcribed chromatin) compared to the rapid clearance of repressive H3K27me3 modifications over the same chromatin territory ($n = 2$ replicates, mean ± s.d.). AU, arbitrary units.

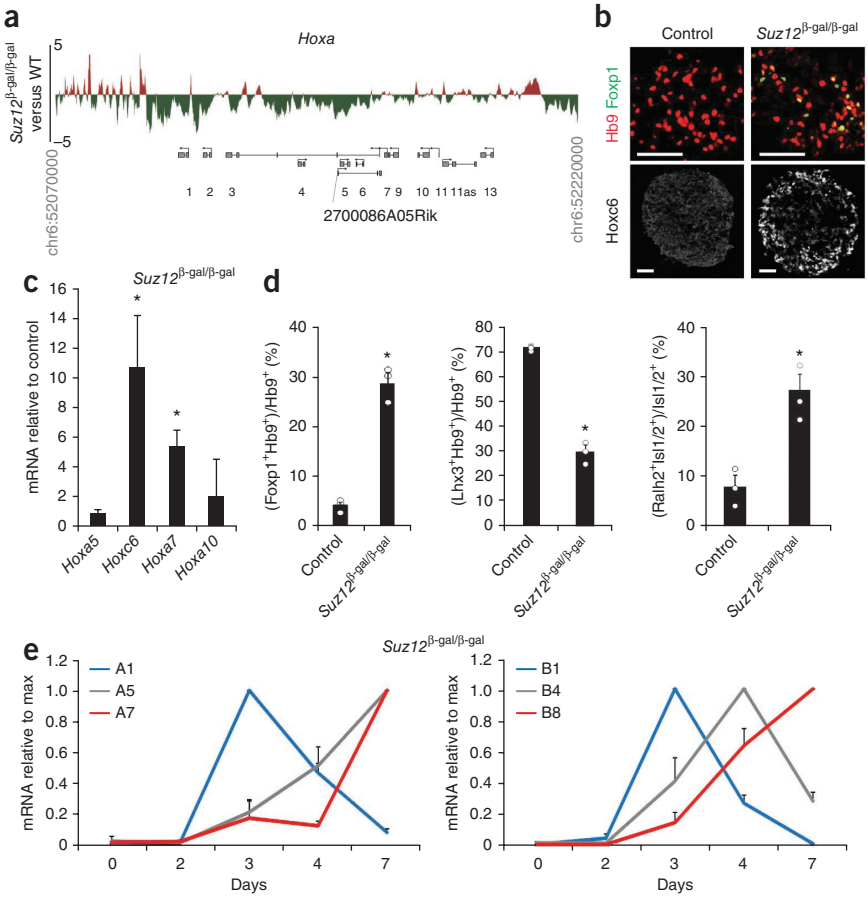

Figure 2 Patterns of *Hox* gene expression in *Suz12*$^{\beta\text{-gal}/\beta\text{-gal}}$ cells differentiated into motor neurons. (**a**) Decreased density of H3K27me3 modification over a 150-kb region spanning the *Hoxa* cluster in *Suz12*$^{\beta\text{-gal}/\beta\text{-gal}}$ ESCs. Positive relative enrichment in H3K27me3 in *Suz12*$^{\beta\text{-gal}/\beta\text{-gal}}$ cells over control cells (wild type, WT) is shown in red, and negative relative enrichment is shown in green. (**b**) A fraction of *Suz12*$^{\beta\text{-gal}/\beta\text{-gal}}$ motor neurons express Hoxc6 and Foxp1, which are markers of brachial spinal motor neurons. Although differentiation of *Suz12*$^{\beta\text{-gal}/\beta\text{-gal}}$ cells was compromised, cells that acquired motor neuron identity (Hb9$^+$) were detected at day 7 of differentiation. Some of the *Suz12*$^{\beta\text{-gal}/\beta\text{-gal}}$ motor neurons acquired expression of a brachial marker, Hoxc6, and a marker of brachial limb-innervating motor neurons, Foxp1. Scale bars, 50 µm. (**c**) Upregulation of brachial *Hox* genes in *Suz12*$^{\beta\text{-gal}/\beta\text{-gal}}$ motor neurons. Quantitative PCR (qPCR) analysis of *Hoxa5*, *Hoxa7*, *Hoxc6* and *Hoxa10* mRNA levels on day 7. The *Hox* mRNA levels in *Suz12* mutant cells were normalized to those of control cells (mean ± s.e.m., $n = 3$ replicates, $^*P < 0.05$ (*t* test)). (**d**) *Suz12*$^{\beta\text{-gal}/\beta\text{-gal}}$ motor neurons acquire a limb-innervating identity. Deregulation of *Hox* gene expression in *Suz12*$^{\beta\text{-gal}/\beta\text{-gal}}$ cells results in a significant increase in the number of Hb9$^+$ motor neurons expressing Foxp1, downregulation of Lhx3 and an increase in the number of Isl1/2$^+$ motor neurons expressing Raldh2 (mean ± s.e.m., $n = 3$ replicates (with each represented by a white circle), $^*P < 0.05$ (*t* test)). (**e**) qRT-PCR analysis of dynamic changes in *Hoxa1* (A1), *Hoxa5* (A5), *Hoxa7* (A7), *Hoxb1* (B1), *Hoxb4* (B4) and *Hoxb8* (B8) transcripts relative to their maximal (max) levels. Shown is an analysis of RNA samples collected at five time points during differentiation of *Suz12*$^{\beta\text{-gal}/\beta\text{-gal}}$ cells, revealing a collinear expression profile of *Hox* genes (mean ± s.e.m., $n = 3$ replicates).

in the maintenance of *Hox* gene expression patterns. ChIP analysis revealed that the density and distribution of H3K27me3 modifications changed markedly during the differentiation of ESCs into motor neurons. Although the *Hox* clusters are covered by a high density of H3K27me3 modifications at the ESC stage, the repressive mark was reduced to background levels in a 3′ *Hox* chromatin domain spanning *Hox1*–*Hox5* in motor neurons at day 7 (**Fig. 1b** and **Supplementary Fig. 1**). The H3K27me3-depleted domain corresponds to the domain bound by RARs after the addition of retinoic acid and harbors all *Hox* genes that are expressed in cervical motor neurons (**Fig. 1b**)[19]. Together these data indicate that large-scale changes in histone modification patterns accompany the differentiation of ESCs into spinal motor neurons of defined rostrocaudal positional identity.

Chromatin-state analysis of mouse embryonic tail buds at different developmental stages suggested a directional and temporally progressive removal of H3K27me3 modifications from *Hox* clusters[14]. To determine the dynamics of H3K27me3 removal during neuronal development, we performed a time-series analysis of histone modifications during ESC differentiation into spinal motor neurons. The density of H3K27me3 modifications over *Hox* chromatin remained high until the addition of patterning signals on day 2 of differentiation (**Fig. 1c** and **Supplementary Fig. 2**). After 1 d of treatment with retinoic acid and SAG (day 3 of differentiation), we observed a domain-wide decrease in the density of H3K27me3 modifications spanning *Hox1*–*Hox5* (**Fig. 1c** and **Supplementary Fig. 2**). By day 4 (the motor neuron progenitor stage), the pattern of H3K27me3 modifications over the *Hox* genes was indistinguishable from that observed in postmitotic motor neurons on day 7 of differentiation (**Fig. 1c** and **Supplementary Fig. 2**). The rapid removal of repressive modifications was driven by retinoic acid treatment. Day-2 embryoid bodies that were treated with retinoic acid for 8 h showed marked loss of repressive modifications in the *Hox1*–*Hox5* domain compared to control untreated cells (**Supplementary Fig. 2**). Analysis of Ring1b and Suz12, components of the polycomb repressive complexes PRC1 (which is involved in chromatin compaction and repression of transcription[26]) and PRC2 (a methyltransferase complex that is required for the maintenance of H3K27me3) revealed that both complexes are rapidly displaced from the activated *Hox* chromatin domains after retinoic acid treatment (**Supplementary Fig. 3**). Together these results indicate that retinoic acid–mediated activation and recruitment of RARs to locations within *Hox1*–*Hox5* chromatin initiates saltatory (rapid, domain-wide) removal of polycomb repressors and H3K27me3 modifications during motor neuron differentiation.

To directly compare the kinetics of H3K27me3 removal with the transcription of *Hox* genes using the same platform, we profiled histone H3 Lys79 dimethylation (H3K79me2) modifications. H3K79me2 modifications are correlated with the presence of an elongating RNA polymerase II complex and can thus be used as a proxy for transcriptional activity[27]. In contrast to the domain-wide changes in H3K27me3 density, a time-series analysis revealed temporally and spatially progressive accumulation of H3K79me2 modifications within the H3K27me3-depleted domain during spinal motor neuron differentiation (**Fig. 1c**). This finding is consistent with the temporally progressive and collinear activation of *Hox* gene expression observed

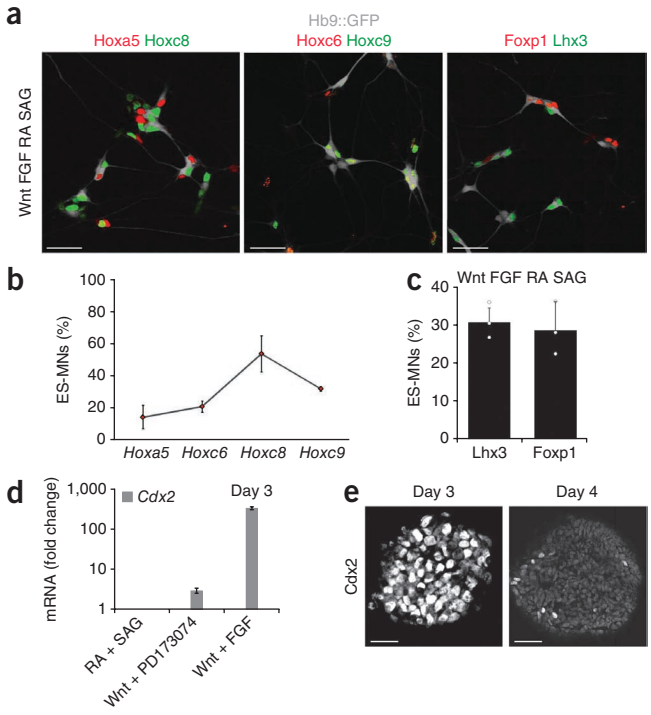

Figure 3 Wnt3A and FGF2 induce Cdx2 and caudalize differentiating motor neurons. (**a**) Wnt3A and FGF2 signaling induce caudal *Hox* gene expression and lateral motor column (LMC) character. Motor neurons from dissociated cell cultures derived from differentiation induced by SAG, retinoic acid, Wnt and FGF were labeled with the *Hb9::GFP* transgene (gray) and stained with antibodies to Hoxa5, Hoxc6 or Foxp1 (red) and Hoxc8, Hoxc9 and Lhx3 (green). Scale bars, 25 µm. (**b**) Quantification of *Hox* gene expression in motor neurons (percentage of Hb9::GFP$^+$ cells). ES-MNs, embryonic stem motor neurons (mean ± s.e.m., $n = 3$ replicates). (**c**) Quantification of the columnar markers Foxp1 and Lhx3 in motor neurons (percentage of Hb9::GFP$^+$ cells) (mean ± s.e.m., $n = 3$ replicates (with each represented by a white circle)). (**d**) The SAG, retinoic acid, Wnt and FGF caudalization protocol induces Cdx2. Blocking FGF activity with the FGF receptor inhibitor PD173074 reduces Cdx2 induction. Shown are *Cdx2* mRNA levels after 24 h of treatment with retinoic acid, SAG, Wnt3a and PD173074 or retinoic acid, SAG, Wnt3a and FGF2 normalized to controls treated with retinoic acid and SAG (day 3 of differentiation) (mean ± s.e.m., $n = 3$ replicates). (**e**) Cdx2 protein expression in differentiating cells 24 (day 3) and 48 (day 4) h after treatment with SAG, retinoic acid, Wnt and FGF. Scale bars (day 3), 20 µm; (day 4), 50 µm.

during motor neuron differentiation (**Supplementary Fig. 2b**) and is reminiscent of the progressive collinear activation of *Hox* gene transcription after treatment of embryonal carcinoma cell lines with retinoic acid[6]. The dichotomy between the dynamics of H3K27me3 and H3K79me2 modifications is best illustrated by a comparison of *Hoxa1* and *Hoxa5*. Whereas the rapid clearance of H3K27me3 from *Hoxa1* coincides with H3K79me2 accumulation, the similarly rapid clearance of H3K27me3 modifications from *Hoxa5* is followed by a delayed, gradual accumulation of H3K79me2 modifications (**Fig. 1d**). On the basis of these observations, we conclude that *Hox* chromatin is partitioned into transcriptionally accessible (H3K27me3-low) and repressed (H3K27me3-high) domains in response to retinoid signaling. The rapid kinetics of H3K27me3 clearance cannot explain the temporally progressive pattern of *Hox* gene transcription, indicating that the clearance of PcG-repressive chromatin modifications is permissive rather than instructive for activation of *Hox* gene expression.

Suz12 activity is required to maintain *Hox* gene repression

To study the role of H3K27me3 modifications, we investigated whether ESCs harboring mutations in key PRC2 components (Eed, Ezh2 and Suz12) can be directed to differentiate into motor neurons *in vitro*. Genetic inactivation of the PRC2 complex leads to the loss of H3K27me3 modifications and early embryonic lethality[28]. Likewise, ESC lines in which PRC2 function is disrupted ($Eed^{-/-}$ or $Ezh2^{-/-}$)[29,30] did not differentiate along a neural lineage. However, we determined that previously reported β-galactosidase (β-gal) gene-trap mutation of *Suz12* (ref. 31) is a hypomorph, and ESCs homozygous for this allele maintain a low amount of H3K27me3 (**Fig. 2a** and **Supplementary Fig. 4**). The hypomorphic line was able to differentiate into motor neurons, although with a lower efficiency (**Fig. 2b**). Analysis of *Hox* gene expression in $Suz12^{\beta\text{-gal}/\beta\text{-gal}}$ ESCs differentiated into cervical spinal motor neurons revealed a significant increase in the expression of the brachial spinal cord *Hox* genes *Hoxc6* and *Hoxa7* (**Fig. 2b**,**c**) as compared to wild-type cells. Consistent with this observation, a subset of differentiated $Suz12^{\beta\text{-gal}/\beta\text{-gal}}$ cells acquired the identity of limb-innervating motor neurons (Foxp1$^+$Raldh2$^+$Lhx3$^-$) that are found in the brachial but not the cervical spinal cord (**Fig. 2b**,**d**). Notably, $Suz12^{\beta\text{-gal}/\beta\text{-gal}}$ mutant cells retained collinear expression of *Hox* genes during motor neuron differentiation (**Fig. 2e**). Together these findings provide evidence that the PRC2 complex is crucial for the maintained repression of *Hox* genes that are located in H3K27me3-high chromatin territory and for proper specification of motor neuron subtype identity.

Wnt3A and FGF2 signals caudalize motor neurons

Our observation that retinoic acid signaling leads to the clearance of repressive chromatin modifications from only a subset of *Hox* genes suggests that other patterning signals might control the removal of H3K27me3 modifications from more caudal *Hox* chromatin domains. To test this hypothesis, we examined mechanisms underlying the specification of more caudal spinal motor neurons. Wnt and FGF patterning signals are necessary for the specification of brachial and thoracic motor neurons expressing Hox6–Hox9 transcription factors[16] and are sufficient to induce caudal spinal *Hox* gene expression in chick neural tube explants[17]. We systematically optimized caudalization of differentiating ESCs by treatment with Wnt3A and FGF2 and identified conditions (150 ng ml^{-1} Wnt3a and 100 ng ml^{-1} FGF2) that gave rise to a mixture of motor neurons expressing the thoracic marker Hoxc9 (28.9 ± 3.1% (mean ± s.e.m.) of all motor neurons) and the brachial markers Hoxc6 (20.8 ± 2.4% of all motor neurons) and Hoxc8 (50.4 ± 7.1% of all motor neurons), as well as the limb-innervating motor neuron marker Foxp1 (28.6 ± 3.9% of all motor neurons)[32,33] (**Fig. 3a**–**c**).

To identify transcription factors that mediate the induction of *Hox6*–*Hox9* by extrinsic Wnt and FGF signals, we focused on the evolutionarily conserved family of Cdx transcription factors that are necessary for the development of caudal structures[18,34]. Of the three mammalian Cdx homologs, Cdx2 showed the greatest degree of upregulation (336-fold ± 22-fold (mean ± s.e.m.)) at 24 h after treatment with SAG, retinoic acid, Wnt and FGF (**Fig. 3d**). Activation of Cdx2 expression was dependent on a synergistic action of Wnt and FGF, as treatment of cells with Wnt3A[16] or FGF2 alone did not induce high levels of Cdx2 expression (**Fig. 3d** and **Supplementary Fig. 5**). Cdx2 protein expression was transient, dropping to basal levels by 48 h after the beginning of treatment (**Fig. 3e**). These results raise the possibility that transiently expressed Cdx2 might mediate the synergistic caudalizing activity of Wnt and FGF signals and regulate *Hox* gene expression.

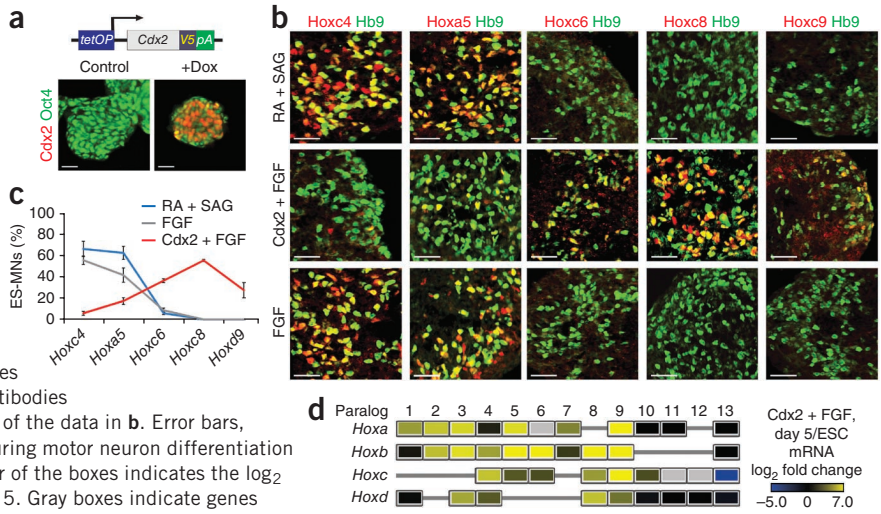

Figure 4 Cdx2 induces caudal *Hox* gene expression during motor neuron differentiation. (**a**) Diagram of an inducible V5-tagged Cdx2 ESC construct (iCdx2). Shown are control and induced iCdx2 ESCs stained with antibodies to Cdx2 (red) and Oct4 (green), demonstrating that tagged Cdx2 is able to repress Oct4 expression. tetOP, tetracycline operator; V5, V5 epitope tag; pA, polyadenylation signal. Scale bars, 20 μm. (**b**) The expression of Cdx2 in combination with FGF2 treatment induces caudal *Hox* gene expression during motor neuron differentiation. Day-7 cultures from the groups treated with SAG and retinoic acid, SAG, retinoic acid, Dox and FGF (Cdx2 + FGF) or SAG, retinoic acid and FGF (FGF) were stained with antibodies to Hoxc4, Hoxa5, Hoxc6, Hoxc8 or Hoxc9 (red) and antibodies to Hb9 (green). Scale bars, 20 μm. (**c**) Quantification of the data in **b**. Error bars, s.e.m.; $n = 3$. (**d**) Expression of *Hox* genes at day 5 during motor neuron differentiation induced by SAG, retinoic acid, Dox and FGF. The color of the boxes indicates the $\log_2$ fold change in signal intensity between ESCs and day 5. Gray boxes indicate genes that are not represented on the GeneChip arrays.

Cdx2 and FGF induce caudal *Hox* expression in motor neurons

To determine whether Cdx2 activity is sufficient to activate caudal *Hox* gene expression independently of Wnt and FGF signaling, we generated a doxycycline (Dox)-inducible V5-tagged Cdx2-expressing ESC line (iCdx2)[25]. The functionality of epitope-tagged Cdx2 is demonstrated by its ability to suppress Oct4 expression after its induction in ESCs[35] (**Fig. 4a**). Next we asked whether the expression of Cdx2 is sufficient to induce caudal *Hox* gene expression in the context of cervical motor neurons differentiated by retinoic acid and SAG. Combined Dox and FGF2 treatment of embryoid bodies also treated with retinoic acid and SAG on day 3 resulted in an efficient induction of Hoxc6, Hoxc8 and Hoxd9 expression (**Fig. 4b–d**). Expression of Cdx2 had no effect on *Hox* gene expression in the presence of the FGF receptor inhibitor PD173074 (**Supplementary Fig. 5b**), and similarly, FGF2 treatment alone was not sufficient to induce caudal *Hox* gene expression (**Fig. 4b,c**).

These results indicate that FGF signaling has a dual role during neural rostrocaudal patterning: first, it synergizes with Wnt to induce Cdx2 expression, and second, it synergizes with Cdx2 to activate caudal *Hox* gene expression.

Cdx2 binds and controls *Hox* chromatin modifications

If Cdx2 regulates *Hox* gene expression directly, it should bind to genomic locations within *Hox* clusters. We performed Cdx2 ChIP sequencing (ChIP-seq) experiments 48 h after Dox treatment and identified 39,493 Cdx2 binding sites ($P < 0.001$; Online Methods), including 118 binding sites within the *Hox* clusters (**Fig. 5a**). The primary DNA sequence motif that was over-represented under the Cdx2 ChIP-seq peaks corresponded to the previously described Cdx2 binding motif GYMATAAA[36] (**Fig. 5b**). Cdx2 selectively binds within the *Hox1–Hox9* paralogous chromatin domains (**Fig. 5c** and **Supplementary Fig. 6**), and the 5′ extent of Cdx2 association with *Hox* chromatin is in register with the last 5′ *Hox* gene (*Hox9* paralogs) induced in caudalized motor neurons (**Fig. 5c** and **Supplementary Fig. 6**). Taken together these results reveal that Cdx2 associates with regulatory regions proximal to transcriptionally active *Hox* genes, suggesting its involvement in the direct regulation of *Hox* gene expression during the specification of brachial and thoracic motor neurons.

To determine whether transient expression of Cdx2 caused changes in PcG-mediated chromatin modifications, we measured the status of H3K27me3 by ChIP-seq analysis 36 h after treatment with Dox and

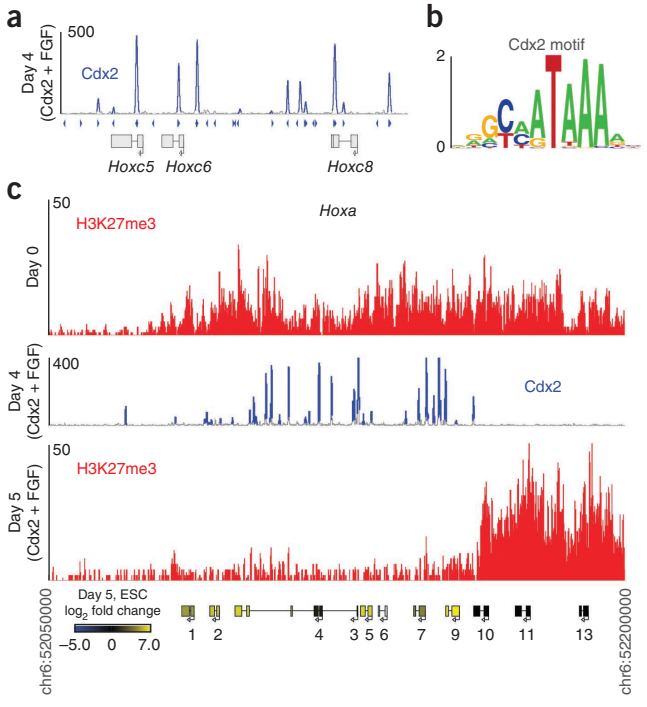

Figure 5 Cdx2 controls *Hox* gene expression and chromatin modifications directly. (**a**) Cdx2 protein associates with *Hox* regulatory regions. The track represents the read count of a Cdx2 ChIP-seq experiment over the 35-kb region of the *Hoxc* cluster. Blue peaks are those significantly enriched over control ($P < 0.001$; Online Methods), suggesting Cdx2 binding. Blue arrowheads under the ChIP-seq track represent the locations of matches to the Cdx2 motif. (**b**) The primary motif enriched under the Cdx2 ChIP-seq peaks. (**c**) The *Hoxa* chromatin boundary is established between *Hoxa9* and *Hoxa10* after Cdx2 induction. The red tracks represent H3K27me3 enrichment over a 150-kb genomic region that includes the *Hoxa* cluster at days 0 (ESC stage) and 5. The center track represents Cdx2 binding on day 4. The blue peaks denote Cdx2 ChIP-seq signals that are significantly enriched above background ($P < 0.001$; Online Methods). The color of the genes indicates the $\log_2$ fold change in signal intensity between ESCs and day 5.

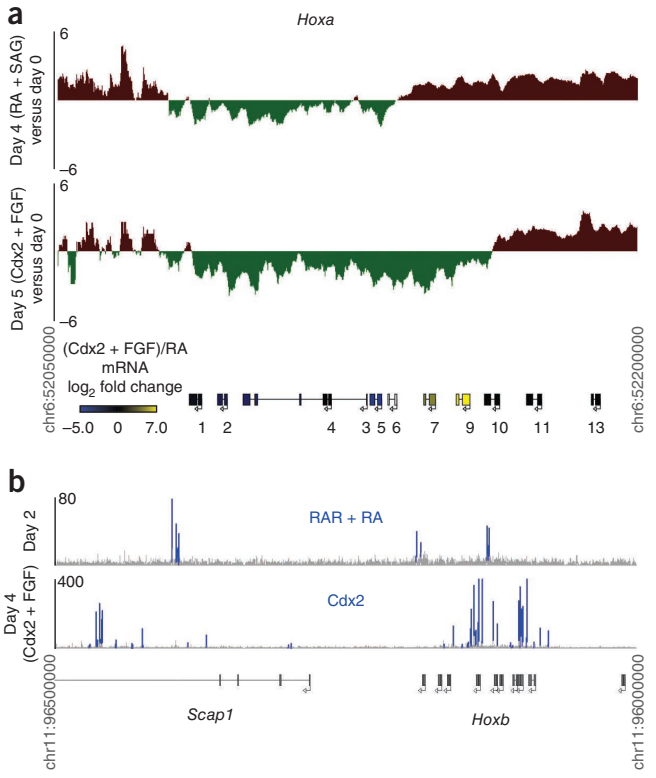

Figure 6 The sequential activity of RAR and Cdx2 establishes two distinct chromatin states. (**a**) Relative changes in H3K27me3 chromatin modifications in the *Hoxa* cluster (150 kb) during cervical and brachial or thoracic motor neuron differentiation. The tracks represent the H3K27me3 enrichment difference between day 0 and day 4 (SAG and retinoic acid treatment) or day 5 (SAG, retinoic acid, Dox and FGF treatment). Positive relative enrichment is shown in dark brown, and negative relative enrichment is shown in green. The color of the genes indicates the $\log_2$ fold change in mRNA levels between the caudal (SAG, retinoic acid, Dox and FGF) and rostral (SAG and retinoic acid) protocols. Gray boxes indicate genes that are not represented on the GeneChip arrays. The repression of rostral *Hox* genes (blue) is concomitant with the upregulation of *Hoxa9* (yellow). (**b**) RAR and Cdx2 associate with local and putative distal regulatory regions. The tracks represent ChIP-seq enrichment levels for RAR (top) and Cdx2 (bottom) over the 500-kb region spanning the *Hoxb* cluster and distal binding sites within the *Scap1* locus. Blue peaks are those that are significantly enriched over control ($P < 0.001$; Online Methods).

FGF (equivalent to 24 h of Cdx2 expression). We observed a domain-wide removal of the repressive histone modifications up to a boundary between the *Hox9* and *Hox10* paralogs (**Fig. 5c** and **Supplementary Fig. 6**). The H3K27me3-depleted domain spans the genomic territory occupied by the Cdx2 transcription factor and harbors *Hox* genes expressed by Cdx2- and FGF2-caudalized motor neurons (**Fig. 5c** and **Supplementary Fig. 6**). These results suggest that, analogous to retinoic acid signaling, transient expression of Cdx2 in neural progenitors results in a global change in the *Hox* chromatin landscape, making a subset of brachial and thoracic *Hox* genes available for transcription in postmitotic spinal motor neurons (**Fig. 6a**).

DISCUSSION

We determined a sequence of molecular events leading from the reception of transient patterning signals to the establishment of lasting rostrocaudal identity in neural tissue. On the basis of the combined analysis of extracellular signals, transcription factors and chromatin states, we conclude that the activity of retinoic acid, Wnt and FGF patterning signals is transmitted by RAR and Cdx2 transcription factors that bind to discrete *Hox* chromatin domains. Transcription factor binding is accompanied by a saltatory clearance of repressive H3K27me3 modifications, partitioning *Hox* clusters into activated and repressed domains. The H3K27me3 pattern is maintained through progenitor cell divisions until the postmitotic motor neuron stage, defining a rostrocaudally appropriate subset of *Hox* genes that are available for the expression and specification of motor neuron subtype identity. Consistent with the notion that patterning signals controlling postmitotic motor neuron *Hox* gene expression act early in development, we recently demonstrated that *Hox* genes are not properly induced during transcriptional programming of motor neurons from ESCs that bypasses neural progenitor stages[37].

Analyses of chromatin states in developing embryos and differentiating ESCs revealed that the temporally progressive activation of *Hox* gene expression is paralleled by a shift of the boundary between H3K27me3-low and -high *Hox* chromatin domains and a visible chromatin decondensation[14,38]. These results suggest two interpretations: the removal of H3K27me3 progresses one gene at a time from the 3′ to the 5′ end of each *Hox* cluster during the period of rostrocaudal patterning, or alternatively, the different observed chromatin states are the product of discrete signaling events acting on distinct *Hox* chromatin domains. The results we present here favor the latter interpretation.

Time-course analysis of changes in *Hox* chromatin modifications revealed a removal of repressive modifications that is rapid (within 24 h after retinoic acid treatment) and that does not progress in a directional 3′-to-5′ manner at the time scale examined (**Supplementary Fig. 2**). Notably, the kinetics of H3K27me3 removal does not correlate with progressive upregulation of *Hox1–Hox5* gene expression over a 4-d period. We propose that what seems to be progressive directional removal of repressive modifications from *Hox* chromatin *in vivo* is actually an effect of sequentially acting patterning signals, each initiating clearance of H3K27me3 modifications from a different subdomain of *Hox* chromatin. Early in development, retinoids activate the rostral *Hox1–Hox5* domain that is expressed in the hindbrain and cervical spinal cord. Later, specified brachial and thoracic segments are exposed to Wnt and FGF signals emanating from the node region[17], leading to Cdx2 induction and activation of the more posterior *Hox6–Hox9* domains. We speculate that other combinations of signals, including FGFs and growth differentiation factor 11 (Gdf11)[5,39], may be involved in activation of the *Hox10–Hox13* chromatin domain.

The rapid removal of H3K27me3 modifications is probably accompanied by relaxation of *Hox* chromatin and large-scale chromatin remodeling[40]. We found that the PRC1 protein Ring1b (**Supplementary Fig. 3**), which is necessary for the maintenance of condensed and repressed *Hox* chromatin[26], is rapidly displaced from the activated domain. Thus our data are consistent with the reported formation of differential chromatin boundaries at different developmental times and rostrocaudal spinal cord positions[3,14,41] and with the large-scale remodeling of *Hox* chromatin observed by fluorescence *in situ* hybridization[10,26,38].

Maintenance of H3K27me3-high domains is necessary for the stable repression of *Hox* genes. Whereas complete clearance of H3K27me3 modifications in Eed- and Ezh2-null ESCs is incompatible with neural differentiation, erosion of H3K27me3 modifications in a Suz12 hypomorph cell line results in a derepression of brachial *Hox* genes in cervical motor neurons. Ectopic expression of *Hoxc6* and *Hoxc7* leads to a change in subtype identity of the resulting motor neurons

and generation of ectopic limb-innervating motor neurons expressing Foxp1. These findings are consistent with the observed derepression of caudal *Hox* genes in polycomb complex mutants[8,9,11], including a recent study that demonstrated that downregulation of the PRC1 gene *Bmi1* in the developing spinal cord *in vivo* leads to a derepression of *Hoxc9* in the brachial spinal cord and a conversion of brachial to thoracic motor neurons[41].

The final expression pattern of *Hox* genes in the nervous system is highly complex and cannot be explained by binary division of *Hox* chromatin into permissive and repressed territories only. Expression of individual *Hox* genes within the permissive chromatin domain is fine tuned by secondary transcriptional interactions. For example, brachial Hox4–Hox8 transcription factors located in the permissive chromatin domain engage in crossrepressive interactions, leading to the diversification of motor neurons into distinct motor pool subtypes[2]. Similarly, the Hoxc9 transcription factor is crucial for direct repression of cervical and brachial *Hox* genes (*Hox1–Hox7*) in permissive chromatin territory, ensuring the generation of motor neurons with proper thoracic identity[3]. Notably, these secondary repressive events do not lead to reacquisition of H3K27me3-repressive polycomb-catalyzed modifications[3] (**Supplementary Fig. 7**).

Expression of *Hox* genes in developing limb mesenchyme is controlled by distal regulatory elements that are brought into physical proximity of *Hox* genes by chromatin looping[42]. However, the transcription factors binding the distal regulatory elements have not been identified, and the mechanisms through which these elements are recruited to the proximity of selected *Hox* genes remain unknown. We speculate that RAR and Cdx2 transcription factors bound within *Hox* genes might coordinate long-distance chromatin looping and provide the necessary local anchor points to demarcate the precise chromatin domains to be activated during rostrocaudal patterning. Our observation that RAR and Cdx2 transcription factors bind in the vicinity of previously identified distal regulatory elements[42] (**Fig. 6b** and data not shown) raises the possibility that long-distance chromatin looping is based on homotypic RAR-RAR and Cdx2-Cdx2 interactions, which are analogous to the previously described long-distance interactions among chromatin sites occupied by estrogen receptors[43].

On the basis of our studies of cervical and thoracic neural tissue, we propose a four-step model of *Hox* gene regulation during rostrocaudal patterning of the developing neural tube (**Supplementary Fig. 8**). First, patterning signals activate the relevant transcription factors that bind to *cis*-regulatory elements within *Hox* clusters and to distal enhancers, resulting in chromatin looping. Second, the transcription factors recruit transactivators that initiate rapid, domain-wide clearance of repressive H3K27me3 modifications from the bound chromatin domains, leading to chromatin decondensation and transcriptional activation of *Hox* genes. Third, the established permissive and repressive chromatin domains are maintained until the postmitotic stage. Fourth, secondary transcriptional regulations of individual *Hox* genes within activated domains lead to the fine-grain patterns of *Hox* gene expression observed in postmitotic motor neurons.

Together, our data provide insight into the precisely orchestrated interplay between signaling molecules, transcription factors and chromatin modifications that jointly contribute to neural tube patterning. These findings open new approaches for directed differentiation of ESCs to the caudal spinal cord nerve cells by extrinsic signals or forced expression of the Cdx2 transcription factor. The study highlights the utility of ESCs as an optimal system to study mechanisms governing embryonic development, to test the inferred principles and to eventually use the developmental logic for the production of cell types that will advance our understanding of the nervous system in health and disease.

METHODS

Methods and any associated references are available in the online version of the paper.

Note: Any Supplementary Information and Source Data files are available in the online version of the paper.

ACKNOWLEDGMENTS

We thank V. Korinek (Institute of Molecular Genetics, Prague) for purified Wnt3A protein, G. Daley (Harvard Medical School) for the Cdx2 construct, M. Kyba (University of Minnesota) for sharing reagents for construction of the inducible Cdx2 ESC line and T. Jessell (Columbia University) and J. Dasen (New York University) for sharing antibodies and for constructive discussion of our findings. E.O.M. was the David and Sylvia Lieb Fellow of the Damon Runyon Cancer Research Foundation (DRG-1937-07), and this work was supported by The Leona M. and Harry B. Helmsley Charitable Trust, US National Institutes of Health grants P01 NS055923 (D.K.G. and H.W.) and R01 NS058502 and NS078097 (H.W.) and The Richard and Susan Smith Family Foundation, Chestnut Hill, Massachusetts (L.A.B.).

AUTHOR CONTRIBUTIONS

E.O.M., S. Mahony, D.K.G. and H.W. conceived the experiments, analyzed the data and wrote the manuscript. E.O.M. generated and validated inducible cell lines and performed cell differentiations and expression analyses. S. Mahony and C.R. performed all computational and statistical analyses of genomic, expression and sequencing data. M.P. and T.P. performed and optimized caudalization experiments. S.R.T. and L.A.B. performed analysis of Prc2-null and hypomorph cell lines. S. McCuine and R.A.Y. performed ChIP-chip experiments.

COMPETING FINANCIAL INTERESTS

The authors declare no competing financial interests.

1. Ensini, M., Tsuchida, T.N., Belting, H.G. & Jessell, T.M. The control of rostrocaudal pattern in the developing spinal cord: specification of motor neuron subtype identity is initiated by signals from paraxial mesoderm. *Development* **125**, 969–982 (1998).
2. Dasen, J.S., Tice, B.C., Brenner-Morton, S. & Jessell, T.M. A Hox regulatory network establishes motor neuron pool identity and target-muscle connectivity. *Cell* **123**, 477–491 (2005).
3. Jung, H. *et al.* Global control of motor neuron topography mediated by the repressive actions of a single hox gene. *Neuron* **67**, 781–796 (2010).
4. Wu, Y., Wang, G., Scott, S.A. & Capecchi, M.R. Hoxc10 and Hoxd10 regulate mouse columnar, divisional and motor pool identity of lumbar motoneurons. *Development* **135**, 171–182 (2008).
5. Liu, J.P., Laufer, E. & Jessell, T.M. Assigning the positional identity of spinal motor neurons: rostrocaudal patterning of Hox-c expression by FGFs, Gdf11, and retinoids. *Neuron* **32**, 997–1012 (2001).
6. Simeone, A. *et al.* Sequential activation of HOX2 homeobox genes by retinoic acid in human embryonal carcinoma cells. *Nature* **346**, 763–766 (1990).
7. Papalopulu, N., Lovell-Badge, R. & Krumlauf, R. The expression of murine Hox-2 genes is dependent on the differentiation pathway and displays a collinear sensitivity to retinoic acid in F9 cells and *Xenopus* embryos. *Nucleic Acids Res.* **19**, 5497–5506 (1991).
8. Akasaka, T. *et al.* Mice doubly deficient for the polycomb group genes Mel18 and Bmi1 reveal synergy and requirement for maintenance but not initiation of Hox gene expression. *Development* **128**, 1587–1597 (2001).
9. Beuchle, D., Struhl, G. & Muller, J. Polycomb group proteins and heritable silencing of *Drosophila* Hox genes. *Development* **128**, 993–1004 (2001).
10. Chambeyron, S. & Bickmore, W.A. Chromatin decondensation and nuclear reorganization of the HoxB locus upon induction of transcription. *Genes Dev.* **18**, 1119–1130 (2004).
11. Boyer, L.A. *et al.* Polycomb complexes repress developmental regulators in murine embryonic stem cells. *Nature* **441**, 349–353 (2006).
12. Bernstein, B.E. *et al.* A bivalent chromatin structure marks key developmental genes in embryonic stem cells. *Cell* **125**, 315–326 (2006).
13. Rinn, J.L. *et al.* Functional demarcation of active and silent chromatin domains in human HOX loci by noncoding RNAs. *Cell* **129**, 1311–1323 (2007).
14. Soshnikova, N. & Duboule, D. Epigenetic temporal control of mouse Hox genes *in vivo*. *Science* **324**, 1320–1323 (2009).
15. Kashyap, V. & Gudas, L.J. Epigenetic regulatory mechanisms distinguish retinoic acid–mediated transcriptional responses in stem cells and fibroblasts. *J. Biol. Chem.* **285**, 14534–14548 (2010).
16. Peljto, M., Dasen, J.S., Mazzoni, E.O., Jessell, T.M. & Wichterle, H. Functional diversity of ESC-derived motor neuron subtypes revealed through intraspinal transplantation. *Cell Stem Cell* **7**, 355–366 (2010).

17. Nordström, U., Maier, E., Jessell, T.M. & Edlund, T. An early role for WNT signaling in specifying neural patterns of Cdx and Hox gene expression and motor neuron subtype identity. *PLoS Biol.* **4**, e252 (2006).
18. Bel-Vialar, S., Itasaki, N. & Krumlauf, R. Initiating Hox gene expression: in the early chick neural tube differential sensitivity to FGF and RA signaling subdivides the HoxB genes in two distinct groups. *Development* **129**, 5103–5115 (2002).
19. Mahony, S. *et al.* Ligand-dependent dynamics of retinoic acid receptor binding during early neurogenesis. *Genome Biol.* **12**, R2 (2011).
20. Shimizu, T., Bae, Y.K. & Hibi, M. Cdx-Hox code controls competence for responding to Fgfs and retinoic acid in zebrafish neural tissue. *Development* **133**, 4709–4719 (2006).
21. Skromne, I., Thorsen, D., Hale, M., Prince, V.E. & Ho, R.K. Repression of the hindbrain developmental program by Cdx factors is required for the specification of the vertebrate spinal cord. *Development* **134**, 2147–2158 (2007).
22. Chawengsaksophak, K., de Graaff, W., Rossant, J., Deschamps, J. & Beck, F. Cdx2 is essential for axial elongation in mouse development. *Proc. Natl. Acad. Sci. USA* **101**, 7641–7645 (2004).
23. Taylor, J.K., Levy, T., Suh, E.R. & Traber, P.G. Activation of enhancer elements by the homeobox gene Cdx2 is cell line specific. *Nucleic Acids Res.* **25**, 2293–2300 (1997).
24. Wichterle, H., Lieberam, I., Porter, J.A. & Jessell, T.M. Directed differentiation of embryonic stem cells into motor neurons. *Cell* **110**, 385–397 (2002).
25. Mazzoni, E.O. *et al.* Embryonic stem cell–based mapping of developmental transcriptional programs. *Nat. Methods* **8**, 1056–1058 (2011).
26. Eskeland, R. *et al.* Ring1B compacts chromatin structure and represses gene expression independent of histone ubiquitination. *Mol. Cell* **38**, 452–464 (2010).
27. Krogan, N.J. *et al.* The Paf1 complex is required for histone H3 methylation by COMPASS and Dot1p: linking transcriptional elongation to histone methylation. *Mol. Cell* **11**, 721–729 (2003).
28. Surface, L.E., Thornton, S.R. & Boyer, L.A. Polycomb group proteins set the stage for early lineage commitment. *Cell Stem Cell* **7**, 288–298 (2010).
29. Montgomery, N.D. *et al.* The murine polycomb group protein Eed is required for global histone H3 lysine-27 methylation. *Curr. Biol.* **15**, 942–947 (2005).
30. Shen, X. *et al.* EZH1 mediates methylation on histone H3 lysine 27 and complements EZH2 in maintaining stem cell identity and executing pluripotency. *Mol. Cell* **32**, 491–502 (2008).
31. Pasini, D., Bracken, A.P., Hansen, J.B., Capillo, M. & Helin, K. The polycomb group protein Suz12 is required for embryonic stem cell differentiation. *Mol. Cell Biol.* **27**, 3769–3779 (2007).
32. Rousso, D.L., Gaber, Z.B., Wellik, D., Morrisey, E.E. & Novitch, B.G. Coordinated actions of the forkhead protein Foxp1 and Hox proteins in the columnar organization of spinal motor neurons. *Neuron* **59**, 226–240 (2008).
33. Dasen, J.S., De Camilli, A., Wang, B., Tucker, P.W. & Jessell, T.M. Hox repertoires for motor neuron diversity and connectivity gated by a single accessory factor, FoxP1. *Cell* **134**, 304–316 (2008).
34. Moreno, E. & Morata, G. Caudal is the Hox gene that specifies the most posterior Drosophile segment. *Nature* **400**, 873–877 (1999).
35. Niwa, H. *et al.* Interaction between Oct3/4 and Cdx2 determines trophectoderm differentiation. *Cell* **123**, 917–929 (2005).
36. Berger, M.F. *et al.* Variation in homeodomain DNA binding revealed by high-resolution analysis of sequence preferences. *Cell* **133**, 1266–1276 (2008).
37. Mazzoni, E.O. *et al.* Synergistic recruitment of transcription factors to cell type specific enhancers programs motor neuron identity. *Nat. Neurosci.* doi:10.1038/nn.3467 (21 July 2013).
38. Chambeyron, S., Da Silva, N.R., Lawson, K.A. & Bickmore, W.A. Nuclear re-organisation of the Hoxb complex during mouse embryonic development. *Development* **132**, 2215–2223 (2005).
39. Liu, J.P. The function of growth/differentiation factor 11 (Gdf11) in rostrocaudal patterning of the developing spinal cord. *Development* **133**, 2865–2874 (2006).
40. Bickmore, W.A., Mahy, N.L. & Chambeyron, S. Do higher-order chromatin structure and nuclear reorganization play a role in regulating Hox gene expression during development? *Cold Spring Harb. Symp. Quant. Biol.* **69**, 251–257 (2004).
41. Golden, M.G. & Dasen, J.S. Polycomb repressive complex 1 activities determine the columnar organization of motor neurons. *Genes Dev.* **26**, 2236–2250 (2012).
42. Montavon, T. *et al.* A regulatory archipelago controls Hox genes transcription in digits. *Cell* **147**, 1132–1145 (2011).
43. Fullwood, M.J. *et al.* An oestrogen-receptor-α–bound human chromatin interactome. *Nature* **462**, 58–64 (2009).

ONLINE METHODS

Cell culture and motor neuron differentiation. Hb9::GFP (HBG3), *Suz12*$^{\beta\text{-gal}/\beta\text{-gal}}$ and Eed mutant ESCs were differentiated as previously described[11,24,31]. Briefly, ESCs were trypsinized and seeded at 5×10^5 cells ml^{-1} in ANDFK medium (advanced Dulbecco's Modified Eagle Medium and F12: neurobasal medium (1:1), 10% knockout serum replacement, penicillin and streptomycin, 2 mM L-glutamine and 0.1 mM 2-mercaptoethanol) to initiate the formation of embryoid bodies (day 0). The medium was exchanged on days 1, 2 and 5 of differentiation. Patterning of embryoid bodies was induced by supplementing the medium on day 2 with 1 μM all-*trans* retinoic acid (Sigma) and 0.5 μM SAG (SAG, Calbiochem). For Wnt and FGF differentiation of ESCs, 150 ng ml^{-1} Wnt3A (R&D Systems) and 100 ng ml^{-1} basic FGF (bFGF; PeproTech) were added along with retinoic acid and SAG on day 2. To generate caudal brachial and thoracic embryonic stem motor neurons using inducible *Cdx2* and FGF, iCdx2-V5 ESCs were induced to differentiate on day 2 with retinoic acid and SAG. On day 3, cultures were treated with Dox (2 μg ml^{-1}) for 6–8 h. Cultures were collected, washed with PBS and treated with 100 nM retinoic acid, 100 ng ml^{-1} FGF and 100 nM SAG, and the medium was changed on day 5. For ChIP experiments, the same conditions were used but were scaled to seed 1×10^7 cells on day 0. All differentiation was performed multiple times analyzing at least three healthy cultures. $n = 1$ equals an independent biological replicate. The data distribution was assumed to be normal, but this was not formally tested. No statistical methods were used to predetermine sample sizes, but our sample sizes were similar to those generally used in the field.

Immunocytochemistry. Embryoid bodies were fixed with 4% paraformaldehyde in PBS, embedded in optimal cutting temperature (OCT) compound (Tissue-Tek) and sectioned for staining using the following conditions: 24 h at 4 °C for primary antibodies and 4 h at room temperature for secondary antibodies. After staining, samples were mounted with Aqua Poly Mount (Polyscience). Images were acquired with an LSM 510 Carl Zeiss confocal microscope. The antibodies used in this study were: goat anti-Oct3 and -Oct4 (ab27985, Abcam, 1:500), mouse monoclonal anti-Cdx2 (CDX2-88, BioGenex, 1:500), rabbit anti-Sox1 (4194, Cell Signaling, 1:200), mouse anti-Isl1 and mouse anti-Hb9 (Developmental Studies Hybridoma Bank, 1:100), and goat anti-Hoxc6 (Santa Cruz). Rabbit anti-Hoxc4 (1:1,000), guinea pig anti-Hoxa5 (1:1,000), mouse anti-Hoxc8 (1:100), guinea pig anti-Hb9 (1:5,000) and rabbit and guinea pig anti-Foxp1 (1:1,000) were gifts from T. Jessell. Alexa 488–conjugated (A11001 and A11008), FITC-conjugated (715-095-150 and 706-095-148), Cy3-conjugated (715-165-150, 711-165-152 and 706-165-148) and Cy5-conjugated (715-175-150 and 711-175-152) secondary antibodies were used at a dilution of 1:2,000.

Quantifications of embryonic stem motor neuron cultures. To determine motor neuron differentiation efficiency and the fraction of motor neurons expressing each gene, embryoid bodies were dissociated on day 6 of differentiation. On day 7, we examined the number of Hb9$^+$ cells and the total number of DAPI$^+$ cells using immunocytochemistry or the expression of Hoxc8 in post-mitotic Hb9$^+$ embryonic stem motor neurons.

Expression analysis. Total RNA was extracted from ESCs or embryoid bodies using the Qiagen RNAeasy kit. For qPCR analysis, cDNA was synthesized using the SuperScript III system (Invitrogen) and amplified using the SYBR Green brilliant PCR amplification kit (Stratagene) and an Mx3000 thermocycler (Stratagene). For GeneChip expression analysis, RNA was amplified using the Ovation amplification and labeling kit (NuGen) and hybridized to Affymetrix Mouse Genome 430 2.0 microarrays. Expression experiments were performed in biological triplicate for each time point analyzed. Arrays were scanned using the GeneChip Scanner 3000. Data analysis was carried out using the affylmGUI BioConductor package[44]. GC robust multiarray (GCRMA) normalization[45] was performed across all arrays, which was followed by linear model fitting using Limma[46]. Differentially expressed genes were defined by ranking all probesets by the moderated *t* statistic–derived *P* value (adjusted for multiple testing using the Benjamini and Hochberg method[47]) and setting thresholds of $P < 0.001$ and fold change ≥2. All arrays were submitted to the US National Institutes of Health (NIH) Gene Expression Omnibus (GEO) database under accession numbers GSE19372 (retinoic acid–dependent and SAG-dependent motor neuron differentiation time series) and GSE39422 (response to Cdx2 expression in motor neuron progenitors).

qPCR primers. The following primers were used for qPCR (forward, reverse): *Cdx1*: ACAGCCGGTACATCACTATCC, CTTGTTTACTTTGC GCTCCTTG; *Cdx2*: TAGTCGATACATCACCATCAGG, TGATTTTCCTC TCCTTGGCTCT; *Cdx4*: GCAATAGATACATCACCATCAGG, ACTTTGCA CGGAACCTCCAG; *Hoxa5*: TGTACGTGGAAGTGTTCCTGTC, GTCACA GTTTTCGTCACAGAGC; *Hoxc6*: TAGTTCTGAGCAGGGCAGGA, CGAG TTAGGTAGCGGTTGAAGT; *Hoxc8*: GTAAATCCTCCGCCAACACTAA, CGCTTTCTGGTCAAATAAGGAT; *Hoxc9*: GCAAGCACAAAGAGGAGAA GG, CGTCTGGTACTTGGTGTAGGG; *HPRT*: AGCAGGTGTTCTAGT CCTGTGG, ACGCAGCAACTGACATTTCTAA; and *B-actin*: TGAGAGGG AAATCGTGCGTGACAT, ACCGCTCGTTGCCAATAGTGATGA.

ChIP-chip protocols. For ChIP experiments, ~3×10^7 cells taken from each developmental time point were crosslinked using formaldehyde and snap frozen in liquid nitrogen. Cells were thawed on ice, resuspended in 5 ml lysis buffer 1 (50 mM 4-(2-hydroxyethyl)-1-piperazineethanesulfonic acid (HEPES)-KOH, pH 7.5, 140 mM NaCl, 1 mM ethylenediaminetetraacetic acid (EDTA), 10% glycerol, 0.5% NP-40 and 0.25% Triton X-100) and mixed on a rotating platform at 4 °C for 5 min. Samples were spun down for 3 min at 3,000 r.p.m., resuspended in 5 ml lysis buffer 2 (10 mM Tris-HCl, pH 8.0, 200 mM NaCl, 1 mM EDTA and 0.5 mM ethylene glycol tetraacetic acid (EGTA)) and mixed on a rotating platform for 5 min at room temperature. Samples were spun down once more, resuspended in lysis buffer 3 (10 mM Tris-HCl, pH 8.0, 100 mM NaCl, 1 mM EDTA, 0.5 mM EGTA, 0.1% Na-deoxycholate and 0.5% N-lauroylsarcosine) and sonicated using a Misonix 3000 model sonicator to sheer crosslinked DNA to an average fragment size of ~500 bp. Triton X-100 was added to the lysate after sonication to a final concentration of 1%, and the lysate was spun down to pellet the cell debris. The resulting whole-cell extract supernatant was incubated on a rotating mixer overnight at 4 °C with 100 μl of Dynal Protein G magnetic beads that had been preincubated for 24 h with 10 μg of the appropriate antibody in a solution of PBS and bovine serum albumin (BSA). The following antibodies were used for ChIP experiments: antibodies to total H3 (Abcam, AB1791), H3K4me3 (Abcam, ab8580), H3K27me3 (Abcam, ab6002), H3K79me2 (Abcam, ab3594) and pan-RAR (Santa Cruz Biotechnology, sc-773). After ~16 h of bead-lysate incubation, beads were collected with a Dynal magnet. ChIP samples probing for transcription factor binding were washed with the following regimen with mixing on a rotating mixer at 4 °C for 5 min per buffer: low-salt buffer (20 mM Tris, pH 8.1, 150 mM NaCl, 2 mM EDTA, 1% Triton X-100 and 0.1% SDS), high-salt buffer (20 mM Tris, pH 8.1, 500 mM NaCl, 2 mM EDTA, 1% Triton X-100 and 0.1% SDS), LiCl buffer (10 mM Tris, pH 8.1, 250 mM LiCl, 1 mM EDTA, 1% deoxycholate and 1% NP-40) and Tris plus EDTA containing 50 mM NaCl. ChIP samples probing for histone and chromatin marks were washed four times with RIPA buffer (50 mM HEPES-KOH, pH 7.6, 500 mM LiCl, 1 mM EDTA, 1% NP-40 and 0.7% Na-deoxycholate) and then once with Tris plus EDTA containing 50 mM NaCl, again mixing on a rotating mixer at 4 °C for 5 min per buffer. After the final bead wash, samples were spun down to collect and discard excess wash solution, and bound antibody-protein-DNA fragment complexes were eluted from the beads by incubation in elution buffer at 65 °C with occasional vortexing. Crosslinks were reversed by overnight incubation at 65 °C. Samples were digested with RNase A and Proteinase K to remove proteins and contaminating nucleic acids, and the DNA fragments were precipitated with cold EtOH. The resulting purified DNA fragments were amplified by ligation-mediated PCR and labeled with a BioPrime CGH Genomic Labeling System (Invitrogen, 18095-011), and the labeled DNA was cohybridized to custom Agilent DNA microarrays.

Array design and hybridization. Labeled DNA samples were cohybridized to custom Agilent DNA microarrays using the Oligo aCGH/ChIP-on-chip Hybridization Kit (Agilent, 5188-5220) at 65 °C for approximately 16 h.

The Agilent 244K probe arrays were designed to tile at least 400 kb surrounding each of the four Hox clusters with an average probe spacing of 110 bp. The remaining probes were used to tile ±30 kb around the TSS of selected genes showing differential patterns of expression during motor neuron differentiation, with probe spacing between 100 bp and 150 bp. The array design and all

ChIP-chip array data have been submitted to the NIH GEO database under accession number GSE19447.

ChIP-chip data analysis. Arrays were scanned at dual photomultiplier tube intensities (10% and 100%) at a 5-μm resolution using an Agilent microarray scanner. Feature extraction was performed with Agilent Feature Extraction software. Background-subtracted values were normalized with (i) median normalization, (ii) line-fitting normalization and (iii) quantile normalization; all normalization code was implemented in SQL as part of our in-house microarray database. Median normalization accounts for differences in the amount of dye hybridized between the two channels. This normalization multiplied the immunoprecipitation signal intensities by the median intensity in the control channel divided by the median intensity in the signal channel such that the median intensity of the two channels is the same. Line-fitting normalization is similar to Loess normalization but with a simpler model: it assumes that the bulk of the data should fall along the line $y = x$. Line fitting was performed using linear regression on the immunoprecipitation values as a function of the control and then the data points were rotated such that the resulting line had slope one and intercept zero; this transformation is performed in log space. Finally, to allow for comparisons of probe intensities across time points, arrays were quantile normalized[48]. Heat map–style figures (**Fig. 1c** and **Supplementary Fig. 2**) were generated in MATLAB by plotting the time series of smoothed array probe intensities, where the smoothing was calculated by the average intensities across a sliding window of 500 bp and an offset of 250 bp.

Histone modification quantification. A two-state hidden Markov model was used to find the boundaries of H3K27me3-enriched domains at each time point. The initial probabilities, transition probabilities and Gaussian distributions for each state were estimated using the scaled Baum-Welch learner in the JaHMM Java library (http://www.run.montefiore.ulg.ac.be/~francois/software/jahmm/).

To compare the dynamics of H3K27me3 and H3K79me2 at the promoter regions of *Hox* genes, we calculated the mean intensity of the probes in 1-kb regions centered around the TSS of each gene at each time point. To determine the statistical significance of the differences in observed H3K27me3 and H3K79me2 enrichment levels at individual Hox genes, we inferred the experimental variance for a given enrichment level by modeling mean-variance relationships across experimental replicates for all 1-kb regions represented on the tiling arrays.

To determine whether a linear relationship exists between the dynamics of repressive histone modifications and *Hox* gene transcription after the addition of retinoic acid, we summarized the amount of H3K27me3 present near *Hoxa1–Hoxa5* by taking the average enrichment of the modification in a 4-kb window centered around the TSS for each gene. The H3K27me3 enrichment and expression values (obtained by microarray analysis) were each normalized to the maximal value obtained for each gene over the course of the time series. A standard linear additive regression model was fitted to the H3K27me3-expression pairs for the entire time series using the least-squares method. The coefficient of determination (R^2) for the fit of this model to these data was 0.7307. This may be interpreted as the proportion of variability in the data that is captured by the model. For the entire time series, a linear additive model captures a good portion of the variability in the data, as noted by the observation that the onset of gene transcription occurs simultaneously with the initial domain-wide removal of the repressive mark. We then limited our analysis to only the data obtained after exposure to retinoic acid. The R^2 value for the fit of the model to these data was 0.0874. A much lower portion of the variability in these data is captured by a linear additive model. Thus, there is very little evidence of a linear relationship between H3K27me3 and expression after the initial onset of transcription that follows exposure to retinoic acid.

ChIP-seq protocols. Samples analyzed by ChIP-seq were prepared similarly to the samples analyzed by ChIP-chip except that purified DNA fragments were not amplified using ligation-mediated PCR but were instead processed according to a modified version of the Illumina/Solexa sequencing protocol (Illumina, http://www.illumina.com/pages.ilmn?ID=252). ChIP-seq reads for RAR were aligned to the mouse genome (version mm8) as described previously[19] using Bowtie[49] version 0.9.9.2 with the options -k 2–best. ChIP-seq reads for Cdx2 and H3K27me3 were aligned to the mouse genome (version mm8) using Bowtie version 0.12.5 with the options -q–best–strata -m 1 -p 4–chunkmbs 1024. Only uniquely mapping reads were analyzed further. Multiple hits aligning to an individual nucleotide position are discarded above the level expected at a 10^{-7} probability from a per-base Poisson model of the uniquely mappable portion of the mouse genome. RAR-binding event analysis was performed as described previously[19], and Cdx2-binding event analysis was performed using GPS[50]. Motifs occurring at RAR and Cdx2 peaks were discovered using GimmeMotifs (with settings -w 200 -a large -g mm8 -f 0.5 -l 500), which combines results from the motif finders MDmodule, MEME, GADEM, MotifSampler, trawler, Improbizer, MoAn and BioProspector. Scaling ratios to allow comparison of H3K27me3 enrichment across experiments were determined using a regression analysis of read counts occurring in 10-kb windows along the mouse genome. Raw sequencing data (FASTQ format) were submitted to the NIH GEO and Sequence Read Archive (SRA) database under accession numbers GSE19409 (RAR), GSE39433 (Cdx2 and H3K27me3 in Cdx2-induced cells) and GSE47485 (H3K27me3 for PcG cell lines).

44. Wettenhall, J.M., Simpson, K.M., Satterley, K. & Smyth, G.K. affylmGUI: a graphical user interface for linear modeling of single channel microarray data. *Bioinformatics* **22**, 897–899 (2006).
45. Wu, Z.J., Irizarry, R.A., Gentleman, R., Martinez-Murillo, F. & Spencer, F. A model based background adjustment for oligonucleotide expression arrays. *J. Am. Stat. Assoc.* **99**, 909–917 (2004).
46. Smyth, G.K. Linear models and empirical bayes methods for assessing differential expression in microarray experiments. *Stat. Appl. Genet. Mol. Biol.* **3**, Article3 (2004).
47. Benjamini, Y. & Hochberg, Y. Controlling the false discovery rate: a practical and powerful approach to multiple testing. *J. R. Stat. Soc. Series B Stat. Methodol.* **57**, 289–300 (1995).
48. Bolstad, B.M., Irizarry, R.A., Astrand, M. & Speed, T.P. A comparison of normalization methods for high density oligonucleotide array data based on variance and bias. *Bioinformatics* **19**, 185–193 (2003).
49. Langmead, B., Trapnell, C., Pop, M. & Salzberg, S.L. Ultrafast and memory-efficient alignment of short DNA sequences to the human genome. *Genome Biol.* **10**, R25 (2009).
50. Guo, Y. *et al.* Discovering homotypic binding events at high spatial resolution. *Bioinformatics* **26**, 3028–3034 (2010).